THE JOURNAL OF BIOLOGICAL CHEMISTRY VOL. 281, NO. 27, pp. 18677–18683, July 7, 2006

Kinetic Investigation of *Escherichia coli* RNA Polymerase Mutants That Influence Nucleotide Discrimination and Transcription Fidelity*

Received for publication, January 18, 2006, and in revised form, April 7, 2006 Published, JBC Papers in Press, April 18, 2006, DOI 10.1074/jbc.M600543200

Shannon F. Holmes[‡1], Thomas J. Santangelo[§2], Candice K. Cunningham[‡], Jeffrey W. Roberts[§], and Dorothy A. Erie[‡¶3]

From the [‡]Department of Chemistry and [¶]Curriculum in Applied and Materials Sciences, University of North Carolina, Chapel Hill, North Carolina 27599 and the [§]Department of Molecular Biology and Genetics, Cornell University, Ithaca, New York 14853

Recent RNA polymerase (RNAP) structures led to a proposed three-step model of nucleoside triphosphate (NTP) binding, discrimination, and incorporation. NTPs are thought to enter through the secondary channel, bind to an E site, rotate into a pre-insertion (PS) site, and ultimately align in the catalytic (A) site. We characterized the kinetics of correct and incorrect incorporation for several *Escherichia coli* RNAPs with substitutions in the proposed NTP entry pore (secondary channel). Substitutions of the semi-conserved residue βAsp^{675}, which is >10Å away from these sites, significantly reduce fidelity; however, substitutions of the totally conserved residues βArg^{678} and βAsp^{814} do not significantly alter the correct or incorrect incorporation kinetics, even though the corresponding residues in RNAPII crystal structures appear to be interacting with the NTP phosphate groups and coordinating the second magnesium ion in the active site, respectively. Structural analysis suggests that the lower fidelity of the βAsp^{675} mutants most likely results from reduction of the negative potential of a small pore between the E and PS sites and elimination of several structural interactions around the pore. We suggest a mechanism of nucleotide discrimination that is governed both by rotation of the NTP through this pore and subsequent rearrangement or closure of RNAP to align the NTP in the A site.

High resolution structures of multisubunit RNA polymerases (RNAPs)[4] have offered insight into many of the regulatory stages and conformational changes associated with the transcription cycle (1–14). Multiple structures of both prokaryotic and eukaryotic RNAPs have revealed a funnel-shaped pore (termed the secondary channel) leading from the surface of the enzyme directly to the active site. This channel has been proposed to be the major, and perhaps only, pathway for entry of nucleoside triphosphates (NTPs) to the active site (1–11, 13, 15).

Recent structures of the yeast RNAP II elongation complex revealed that binding of an incorrect NTP for synthesis was at a site (termed the E site) adjacent to the catalytic NTP binding site (termed the A site) with the position of the base in the E site inverted and pointing out into the secondary channel (6). Comparison of structures with the correct and incorrect nucleotides led to the proposal of a two-step model of NTP binding, in which an incoming NTP first binds to the E site and then rotates through a narrow negatively charged pore (13) into the A site where it pairs with the template base (6). An NTP bound in the E site was also suggested to inhibit backtracking (13). This two-step model, however, does not allow for direct base pairing between the incoming NTP and the template base until the incoming NTP is positioned in the active site. Cramer and co-workers (11) observed an NTP analog in a third site in which the incoming NTP was base-paired with the DNA template base but not positioned for catalysis and suggested that this site was a preinsertion (PS) site. They proposed a mechanism similar to that proposed for T7 RNAP (14, 16, 17) in which the incoming NTP binds to the PS site with RNAP in an "open" conformation and then RNAP closes down on the correctly paired NTP to align the NTP in the active (A) site for catalysis (11). Temiakov *et al.* (9) integrated these two models and proposed a three-step mechanism in which the NTP first binds to the E site and then rotates into the PS site, where hydrogen bonding between the bases is checked, before RNAP closes to bring the DNA template base and NTP pair into the A site. This model allows for a check of fidelity before the template strand base and incoming NTP are positioned such that catalysis can occur.

Despite this large amount of structural information, there is no clear biochemical evidence for these proposed mechanisms of nucleotide binding and discrimination. Furthermore, some researchers have proposed that the primary pathway by which NTPs enter into the active site is through the main channel (18–21). To explore the potential role of residues near the active site, particularly those residues that are surface exposed at the junction of the secondary channel and the active site, in nucleotide binding, discrimination, and incorporation, we have investigated the effects of several amino acid substitutions in the β subunit of *Escherichia coli* RNAP on the kinetics of correct and incorrect nucleotide incorporation. The particular substitutions were previously shown to disrupt Q-mediated antitermination both *in vivo* and *in vitro*, although the exact mechanism for such inhibition remains to be determined (22). We demonstrate that one of these mutants (D675Y) dramatically reduces the fidelity of RNAP. Based on our kinetic data and previous studies (6, 9, 11, 23), we suggest a three-step NTP binding model that permits a "double check" of the identity of the NTP before incorporation. This model can be used to further understand the mechanism underlying nucleotide discrimination and fidelity for multisubunit RNAPs.

MATERIALS AND METHODS

Sources of Protein and DNA—His-tagged wild-type RNAP was purified from log phase cells of strain RL916 (gift of R. Landick) as described previously (24, 25). β His_6-C-terminal tagged wild-type and mutant

* This work was supported by National Institutes of Health Grants GM 54316 (to D. A. E.) and GM 21941 (to J. W. R.). The costs of publication of this article were defrayed in part by the payment of page charges. This article must therefore be hereby marked "*advertisement*" in accordance with 18 U.S.C. Section 1734 solely to indicate this fact.

[1] Current address: NIEHS/NIH, P. O. Box 12233, Research Triangle Park, North Carolina 27709.

[2] Current address: Dept. of Microbiology, Ohio State University, 468 Biological Sciences Bldg., 484 West 12th Ave., Columbus, OH 43210-1292.

[3] To whom correspondence should be addressed. Tel.: 919-962-6370; Fax: 919-966-3675; E-mail: derie@unc.edu.

[4] The abbreviations used are: RNAP, RNA polymerase; GMP-CPP, guanosine-5′-[(α,β)-methyleno]triphosphate.

RNAPs were purified from TOM100 as previously described (22). The RNAP preps are greater than 95% pure (no other bands are visible on a SDS-PAGE gel). To test for nuclease contamination, the purified RNAPs were incubated at 37 °C for 1 h with radiolabeled RNA and then assayed by gel electrophoresis. As a control the labeled RNA was incubated in buffer in the absence of RNAP. No significant degradation of the RNA was seen in either the control or the reaction containing RNAP (data not shown), indicating that there is no nuclease contamination. In addition, no GreA, GreB, or NTPase activity was detectable in preparations using this purification procedure. Finally, experiments with wild-type and the Asp^{675} mutant RNAPs were performed with at least two different RNAP preps. The DNA template was prepared from pDE13 (wild-type template) and amplified by PCR (23). It is biotinylated, 540 nucleotides in length, contains the λP_R promoter, and codes for a transcript in which the first cytosine is 25 nucleotides after the start site of transcription (position +25).

In Vitro Transcription Reactions—For the correct incorporation experiments, RNAP (60 nM) and 5′-biotinylated DNA template (60 nM) bound to streptavidin-coated magnetic beads were incubated 10 min at 37 °C in 1× transcription buffer (30 mM HEPES (pH 8.0), 10 mM Mg^{2+} glutamate, 200 mM K^+ glutamate, 25 μg/ml bovine serum albumin, and 1 mM dithiothreitol) to form open complexes. Complexes stalled at +24 were formed by adding 15 μM UTP, 20 μM ATP, and 20 μM [α-^{32}P]GTP (160 Ci/mmol) and incubating at room temperature for 1 min. The complexes were then washed 7–10 times with ice-cold 1× transcription buffer while holding the reaction tube next to a strong magnet to retain the complexes, and then the complexes were resuspended in ice cold 1× transcription buffer and kept on ice until used in the rapid kinetic experiments. The correct incorporation kinetic experiments were performed at room temperature (~23 °C), using a KinTek Rapid Quench Flow apparatus. For each time point, 20 μl of the purified elongation complexes were injected into one reactant loop and 20 μl of CTP into the other reactant loop. The CTP concentrations reported are final concentrations after mixing in the quench flow. The reactants were mixed for the indicated times and subsequently quenched with 0.5 M EDTA. Each time point represents a separate experiment. To assure that the results were not dependent on the length of time the complexes remained on ice, time points were taken in different orders. For the correct incorporation experiments performed with ATP (incorporation at position +26 on the template), experiments were performed as described previously (26). For the misincorporation reactions, the DNA was not bound to beads and transcription was initiated with the addition of NTPs as described above; however, time points were taken starting immediately after the addition of NTPs and quenched at various times in 100% formamide. At designated times during both the misincorporation and correct incorporation reactions, a portion of the elongation complexes was removed and extended to full length by the addition of 1 mM of all four NTPs (chased) to establish that the complexes were still active. To resolve the products at each position on the template, all samples were run on 8 M urea, 20% polyacrylamide gels. For the correct incorporation experiments, the EDTA was removed from the samples with the aid of a magnet as described above, and the products were resuspended in 100% formamide prior to running on the gels.

Quantification of Rate Data—The amount of radioactivity in each lane of the gel was measured on a Amersham Biosciences PhosphorImager and analyzed with ImageQuant software. The percentage of complexes at each position on the template was calculated by dividing the amount of radioactivity in the indicated band by the total amount of radioactivity in all the bands 24 nucleotides in length and longer.

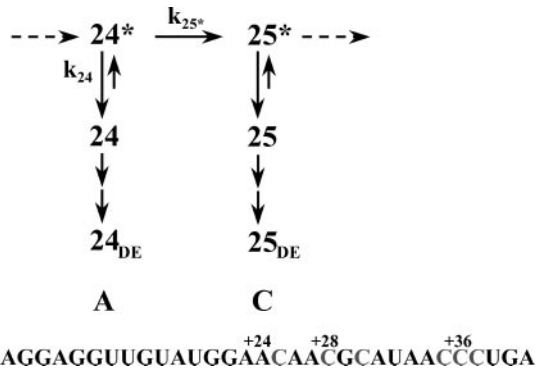

FIGURE 1. **Misincorporation mechanism.** This figure was adapted from Ref. 23. The *numbers* indicate the transcript position on template DE13. (see "Materials and Methods") The corresponding RNA sequence is shown below the figure. *n** and *n* represent the activated and unactivated states, respectively, of an elongation complex at each position, n_{DE} stands for dead-end or arrested complexes. The multiple arrows from *n* to n_{DE} indicate that multiple steps may be involved in the transition from the unactivated state to the arrested state (31).

Determination of Misincorporation Rate Constants—To determine the rate of misincorporation, the misincorporation data were fit to the mechanism described in the text (see Fig. 1) using the kinetics fitting program KinTekSim (27). These data were fit "manually"; that is, the data were simulated using many different combinations of rate constants until the best fits were obtained. The starting points for these values were obtained from the double exponential fits of the data.

RESULTS

All experiments were performed on the DNA template from the plasmid pDE13, which contains the λP_R promoter and initially transcribed sequence shown at the *bottom* of Fig. 1. On this template, the first cytosine to be incorporated is at position +25 (23). By omitting CTP from the initial transcription reaction, misincorporation at position +25 can be monitored (23). Alternatively stable elongation complexes can be stalled at position +24 and purified, and then correct incorporation events can be observed as a function of time.

Correct Incorporation Studies—We investigated the kinetics of correct incorporation of CMP at position +25 and AMP at position +26 (data not shown) for wild-type and four mutants of *E. coli* RNAP. All of the mutant RNAPs have single or double amino acid changes in the β subunit that are in or near the secondary channel. The variants are designated H673L, N620I/D814V, D675Y, and R678C according to the residue(s) that were substituted. The rates of CMP incorporation at low (5 μM) and high (100 μM) [CTP] were measured (Fig. 2). Despite the high degree of conservation among multisubunit RNAPs for several of these residues (Fig. 5*A*), none of the altered RNAPs show a significantly altered incorporation rate at low [CTP] (Fig. 2*A*), and only R678C shows a slightly decreased rate of incorporation at 100 μM CTP (Fig. 2*B*). The most significant difference between the wild-type and mutant RNAPs is that only 70–80% of the wild-type RNAP incorporates CMP within 1 s, whereas ~90% of the variant RNAPs incorporate CMP within 1 s (Fig. 2*A*). We have consistently observed this reduced extent of incorporation with wild-type RNAP, and it is not specific to any particular enzyme preparation (data not shown). The population of complexes that does not go to completion appears to be in backtracked states because given sufficient time these complexes do go to completion (data not shown). This difference suggests that the mutant RNAPs are less prone to enter into backtracked states under these conditions.

Misincorporation Studies of the Variant Enzymes—Previous studies with wild-type RNAP demonstrated that only UMP could be misincorporated in place of CMP (23). To investigate the fidelity of these mutants, we characterized the misincorporation kinetics for each of

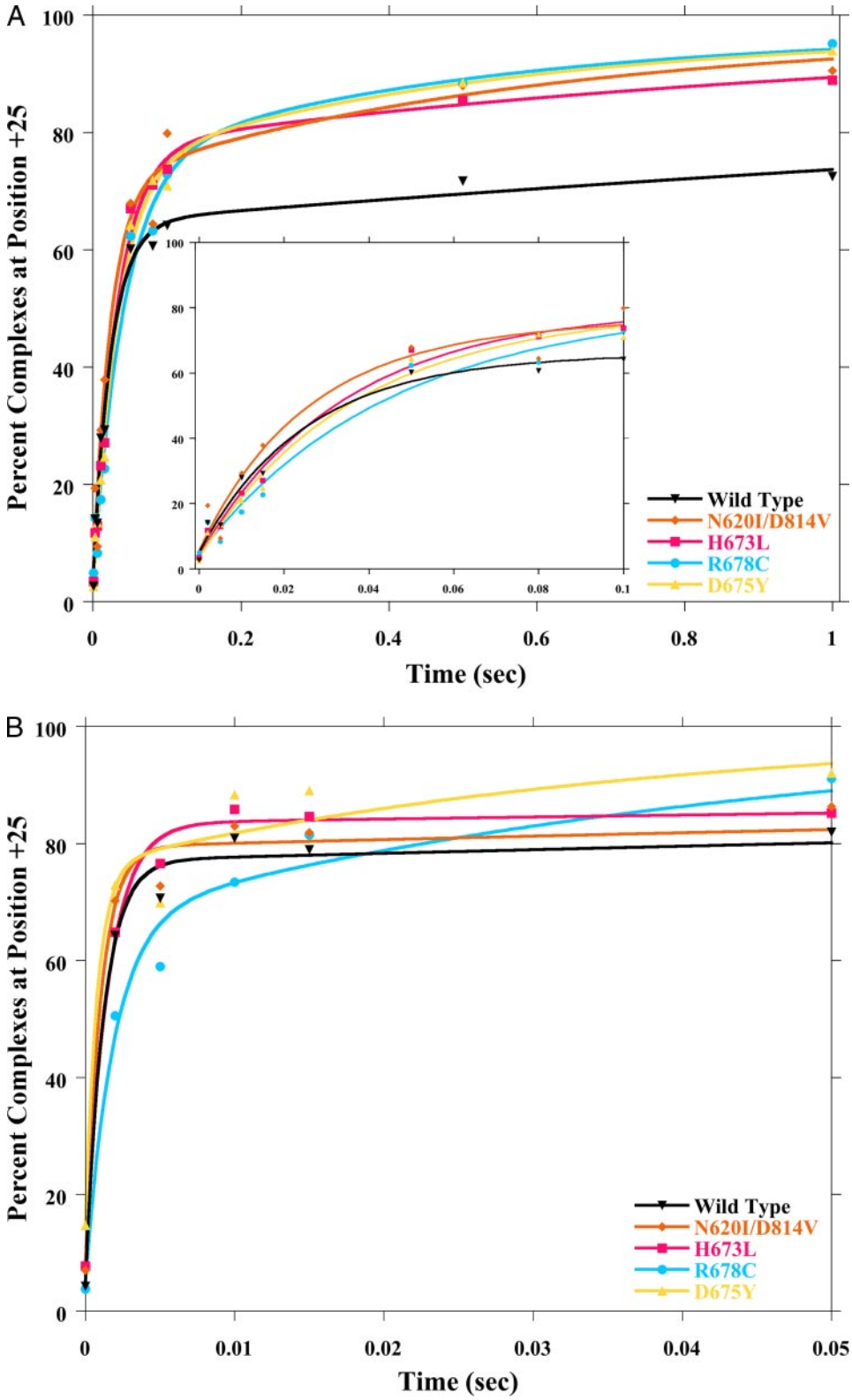

FIGURE 2. **Comparison of correct incorporation kinetics.** The plots show the percentage of complexes at position +25 as a function of time. The curves through the data are double exponential fits. The plots show data from one experiment examining the incorporation of CMP at position +25. However, incorporation of AMP at position +26 was also examined and all rates were similar to wild-type RNAP for all mutant RNAPs (data not shown; see "Materials and Methods"). *A*, incorporation at 5 μM CTP where most synthesis should occur in the unactivated state. The *inset* shows the early time points. A larger percentage of the complexes made with variant polymerases go to completion. *B*, incorporation at 100 μM CTP where most synthesis should occur in the activated state.

these variant RNAPs as well as for wild-type. Fig. 3 shows representative data and fits for the kinetics of misincorporation of UMP for CMP at position +25. The mutants H673L and N620I/D814V behave the same as wild-type, R678C exhibits a slight increase in misincorporation, and D675Y exhibits a dramatic increase in misincorporation (Fig. 3). Specifically, ~80% of the D675Y mutant misincorporates to position +25 (and positions downstream) by 2 min *versus* ~20% for the wild-type (Figs. 3 and 4). Because the rate and extent of misincorporation is increased (Figs. 3 and 4) and the rate of correct incorporation is relatively unchanged (Fig. 2), the fidelity of transcription is specifically reduced with the βD675Y substitution.

The mutation from an aspartic acid to a tyrosine at βAsp^{675} both removes a negative charge and inserts a relatively bulky group. To further elucidate the source of the lower fidelity, we investigated an addi-

tional mutant RNAP in which the aspartic acid at 675 was mutated to a valine (D675V), which is similar in size to the aspartic acid but lacks the charge. Like D675Y, D675V has a significantly increased rate and extent of misincorporation (Fig. 4). These results suggest that the charge on the aspartic acid is important for nucleotide discrimination.

Additionally, our results show that the variant N620I/D814V has no defects with either correct incorporation (Fig. 2) or misincorporation (Fig. 3). βAsp^{814} is invariable, and the corresponding residue in yeast RNAP II (D836 in Rpb2) was observed to be close enough to assist in coordinating a second metal (metal B) in the active site of RNAP II in several crystal structures (2, 6, 28). Asp^{814} does not appear to be essential for coordinating metal B in *E. coli* RNAP because no effect on transcription is observed in the D814V mutant (Figs. 2 and 3). These data are consistent with earlier studies on this mutant (22, 29).

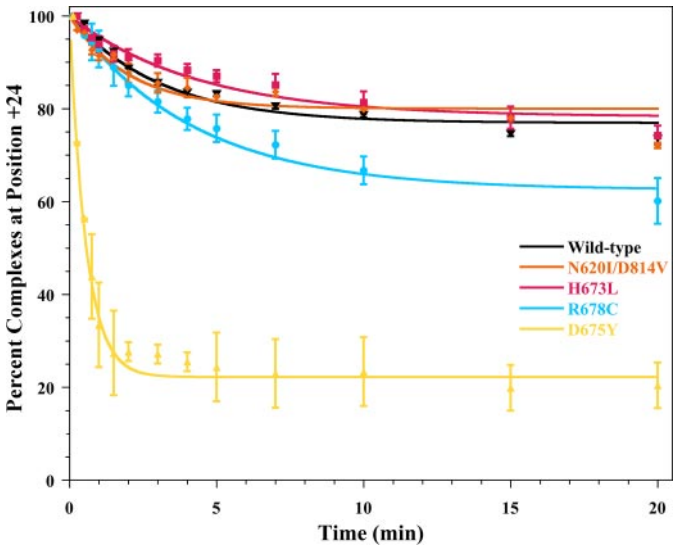

FIGURE 3. **Comparison of misincorporation kinetics.** The plot shows the percentage of complexes at position +24 that elongate (misincorporates at least to position +25) as a function of time. The only variant polymerase that exhibits a significant increase in misincorporation over the wild-type is D675Y. Curves through the data were generated with the program KinSim using the mechanism shown in Fig. 1 and the parameters shown in Table 1 (see "Materials and Methods"). The curves shown are representative data from experiments performed with each polymerase. The *error bars* represent the standard errors in the data over three or more independent experiments.

DISCUSSION

To probe the role of the secondary channel in nucleotide binding and discrimination, we have examined the kinetics of correct and incorrect nucleotide incorporation for several RNAP mutants with changes in conserved and semi-conserved residues (Fig. 5*A*). None of the mutant polymerases exhibit any significant defects in correct incorporation (Fig. 2; data not shown); and only the βAsp^{675} variants exhibit an increase in misincorporation (Figs. 3 and 4). These results indicate that the fidelity (defined as the ratio of rates of correct and incorrect incorporation) of the βAsp^{675} mutants is significantly reduced.

Previous studies of misincorporation demonstrated that the fidelity of transcription is governed, at least in part, by a branched kinetic pathway in which RNAP can switch between two conformational states at each template position (Fig. 1) (23). It was demonstrated that during rapid synthesis, the RNAP ternary complex usually exists in a long lived (half-life of minutes) activated state and that this state decays into an unactivated state if the rate of incorporation is slowed by nucleotide

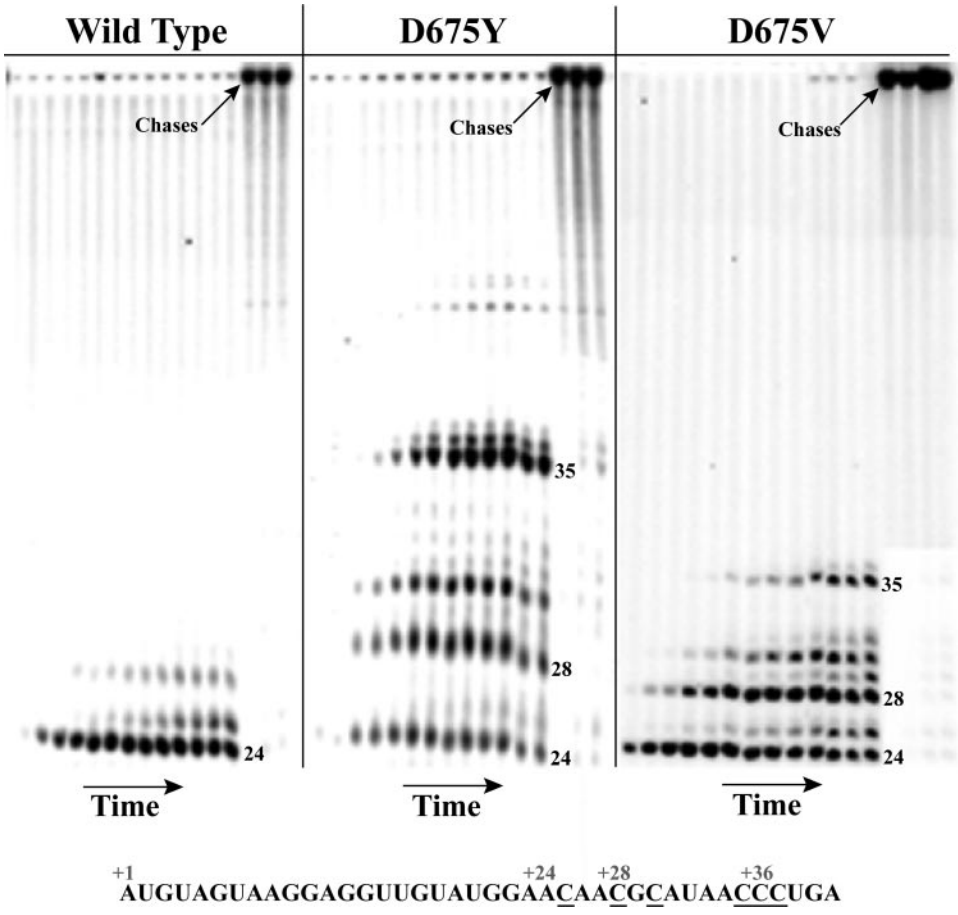

FIGURE 4. **Misincorporation Kinetics of wild-type, D675Y and D675V RNAPs.** Denaturing polyacrylamide gels showing ^{32}-P labeled transcripts generated from each RNAP on DE13 templates (see "Materials and Methods"). Both D675Y and D675V misincorporate to a much higher extent than wild-type RNAP. The length of transcripts is noted to the *right* of each panel. Chase lanes had 1 mM NTPs added to establish that the complexes were still active. The corresponding RNA sequence is shown below the gels. Aliquots of each reaction were removed and quenched at 0.12, 0.25, 0.5, 0.75, 1, 1.5, 2, 3, 4, 5, 7, 10, 15, and 20 min. NTPs were added at time 0.

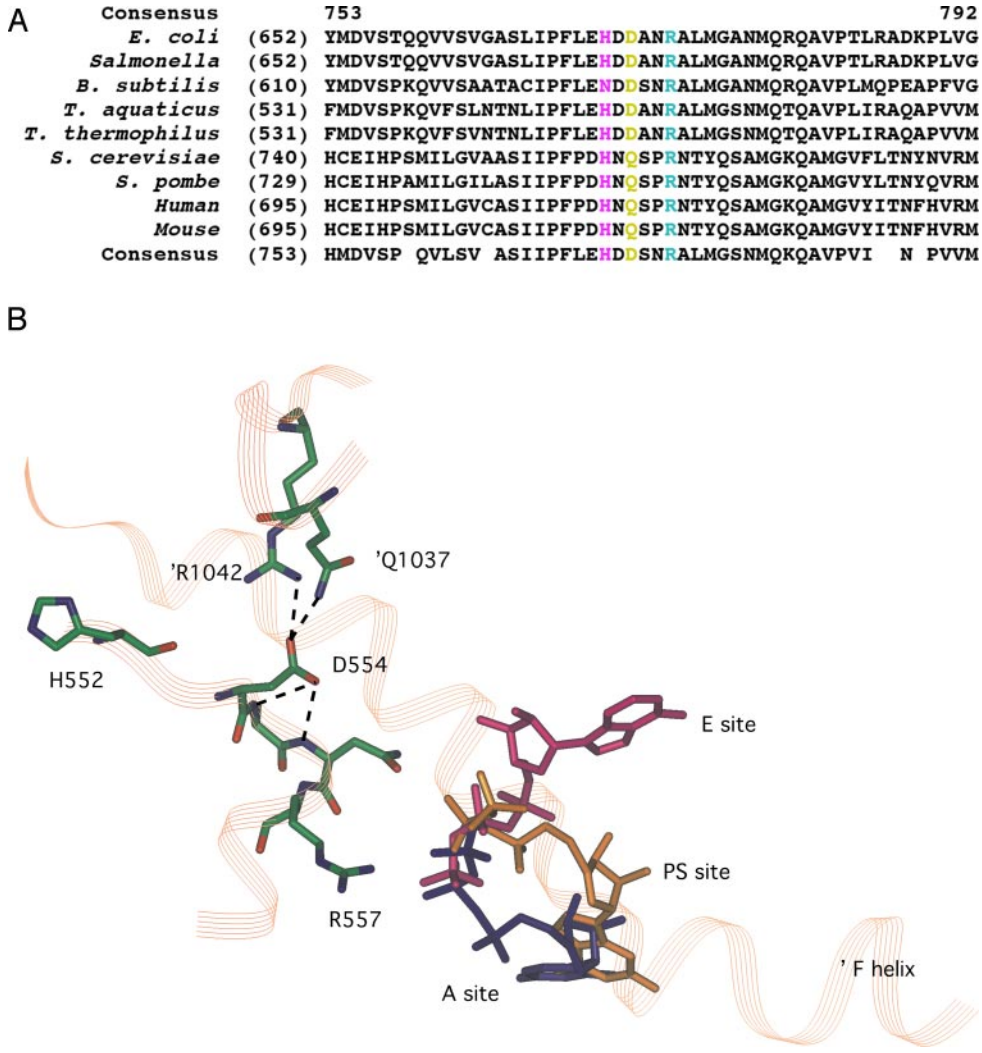

FIGURE 5. **Sequence and structural alignment of the β subunit.** *A*, residues surrounding βAsp^{675} (*shaded* in *yellow*) in *E. coli* are shown. βAsp^{675} is completely conserved in prokaryotes and aligns structurally with a completely conserved glutamine in the eukaryotic RNAPs. The conserved arginine βArg^{678} that interacts with the phosphates of an NTP bound at the E, PS, and A sites is shaded in *cyan*. βHis^{673} is *shaded* in *pink*. The alignments are based on overlays of the *Saccharomyces cerevisiae* RNAP II and *T. aquaticus* RNAP structures and differ from published alignments generated using Blast (2). *B*, model of mutated region with NTPs in the A, PS, and E sites. The region containing three of the mutations investigated (*E. coli* β residues Arg^{678}, His^{673}, and Asp^{675}) is overlaid with RNAP II structures containing a UTP in the A site, an ATP in the E site (6), and a GTP analog, GMP-CPP in the PS site (11). The protein structure shown is *T. aquaticus* β residues 551–561, β′ residues 1037–1045, and the F helix of β′. The numbering is for *T. aquaticus* RNAP; the corresponding residues in *E. coli* for β residues His^{552}, Asp^{554}, and Arg^{557} are His^{673}, Asp^{675}, and Arg^{678}, respectively (see Fig. 5*A*) and for β′ residues Gln^{1037} and Arg^{1042} are Gln^{739} and Arg^{744}, respectively. The NTPs bound in the E, PS, and A sites are shown in *magenta*, *gold*, and *blue*, respectively. The potential salt bridges and hydrogen bonds being made by βAsp^{554} (βAsp^{675} in *E. coli*) are shown as *dashed lines*. The model was generated by superimposing yeast RNAP II Rpb2 residues 760–770 from three crystal structures: one containing a UTP in the active site (A site), one containing an incorrectly matched ATP in the E site (6), and one containing GMP-CPP in the PS site (11) onto *T. aquaticus* β residues 551–561 (*E. coli* β residues 672–682) (1).

depletion (23) (or potentially by a physical block to elongation or a regulatory signal) (23, 30, 31). We have previously proposed a structural model for these states (see Figs. 7 and 8 of Ref. 26). We suggested that the activated state represents RNAPs that exist predominantly in the post-translocated state with NTPs entering the active site through the secondary channel; whereas the unactivated state represents RNAPs that exist predominately in the pretranslocated state, with a possible equilibrium between the pre- and post-translocated states, and that NTPs may enter through the main channel or through the secondary channel in the unactivated state (26). RNAP can catalyze correct incorporation in the unactivated state but at a slower rate than in the activated state (26, 30). In contrast, misincorporation occurs only when RNAP is in the activated state, making the activated state a lower fidelity state than the unactivated state (23, 30, 31). Within the context of this kinetic mechanism, the two ways that misincorporation can be increased are (i) by decreasing the rate of decay (k_{24}) from the activated state to the unactivated, higher fidelity state or (ii) by creating a problem with nucleotide discrimination and thereby increasing the rate of misincorporation in the activated state (k_{25*}) (Fig. 1). Fitting the data to the first step in this misincorporation mechanism reveals that the rate of decay from the activated to the unactivated state (k_{24}) for βD675Y is not significantly different from wild-type RNAP; whereas the rate of misincorporation in the activated state (k_{25*}) is significantly increased (>20-fold) (Table 1). These results indicate that the increased extent of misincorporation

TABLE 1
Rates of misincorporation for variant and wild-type polymerases
These rates were obtained by fitting the data by hand in KinSim using the mechanism shown in Fig. 1 (see "Materials and Methods"). The rates from the double exponential fits were used as starting points for determining the final rates. k_{25*} and k_{24} represent the rate of misincorporation in the activated state and the rate of decay to the unactivated state, respectively.

Polymerase	k_{25*}	k_{24}
	min^{-1}	min^{-1}
Wild-type	0.075	0.25
N620I/D814V	0.1	0.4
R678C	0.09	0.15
H673L	0.05	0.18
D675Y	**1.4**	0.4

relative to wild-type is a result of more rapid incorporation of the incorrect base (k_{25*} (D675Y) > k_{25*} (wild-type)) as opposed to a slower decay into the unactivated state (k_{24} (D675Y) ≈ k_{24} (wild-type)). The increase in k_{25*}, in conjunction with the unaltered rate of correct incorporation, indicates that nucleotide discrimination in the βD675 mutants is compromised.

Previous kinetic studies of misincorporation demonstrated that the rate-limiting step to incorporation of incorrect nucleotides in the activated state is a conformational change prior to bond formation (23), although the nature of this change is unknown. Consequently, βAsp^{675} likely influences this rate-limiting conformational change. Inspection of

the *Thermus aquaticus* and *Thermus thermophilus* RNAP crystal structures (1, 8, 9) with an NTP modeled in the active site reveals that βAsp^{675} (βAsp^{554} in *T. aquaticus*) lies on the surface of the secondary channel and is >15 Å away from the nucleotide base and >10 Å away from the nearest phosphate group, indicating that the loss of nucleotide discrimination in these mutants is very unlikely to be the result of the removal of a direct interaction with the NTP in the active site. An alignment of the RNAP II structures containing NTPs bound in the E, PS, and A sites (as discussed above) with *T. aquaticus* RNAP (1, 6, 11) reveals that the residue corresponding to βD675 (*E. coli*) in eukaryotic RNAP II is a conserved glutamine (Rpb2 subunit, residue Gln^{763}), which is three residues from a totally conserved arginine (Arg^{766} in RNAP II and Arg^{678} in *E. coli*) (Fig. 5). This conserved arginine interacts with the phosphates of the incoming NTP when it is bound in the E, PS, or A sites (1, 6, 9, 11) (Fig. 5). This observation suggests that the lower fidelity of the βAsp^{675} mutants could result from changes in conformation of the E, PS, or A sites by altering the position of Arg^{678}; however, mutation of the conserved Arg^{678} to cysteine, which directly alters this phosphate interaction, exhibits only slightly altered elongation kinetics (Figs. 2 and 3), indicating that this explanation is insufficient to account for the lowered fidelity of the βAsp^{675} mutants.

A close inspection of this region shows that βAsp^{675} (βAsp^{554} in *T. aquaticus*) is at the beginning of a 3-residue β-turn and that one of the side chain oxygens is within hydrogen bonding distance to the backbone nitrogens of the first two residues in the turn (A555 and N556 in *T. aquaticus*) (1) (Fig. 5*B*). In addition, the other oxygen is positioned to form a hydrogen bond and a salt bridge with β′ residues Gln^{1037} and Arg^{1042} in *T. aquaticus* (Gln^{739} and Arg^{744} in *E. coli*), respectively. This network of interactions presumably stabilizes the β-turn and anchors it to the side of the secondary channel (1) (Fig. 5*B*). Although the overall backbone structure of RNAP II is essentially the same as *T. aquaticus* and *T. thermophilus* RNAP in this region, Rpb2 Gln^{763} is not positioned to form equivalent interactions in RNAP II. Instead, Gln^{763} is in a *cis*-proline turn and the turn interacts with the bridge or F-helix rather than the wall of the secondary channel (2, 3, 11). The bridge helix has been observed in at least two configurations (bent and straight) (1, 8, 9), and oscillation between these two configurations has been proposed to be involved in both catalysis and translocation of multisubunit RNAPs (9, 26, 32). Although we cannot rule out the possibility that substitutions at βAsp^{675} alter the conformation or potential for oscillations of the bridge helix, it is unlikely that the substitutions examined here would either increase or decrease the potential for meaningful contacts with the bridge helix in *E. coli* RNAP, and the β-turn is not interacting with the bridge helix in either the *T. aquaticus* or *T. thermophilus* crystal structures (1, 8).

In prokaryotes, substitution of this aspartic acid with a tyrosine or valine would remove the hydrogen bond and salt bridge to β′ as well as the hydrogen bonding interactions that stabilize the β-turn (Fig. 5*B*), thereby changing the surrounding structure and potentially creating a looser configuration in the tunnel around the small pore that separates the E and PS sites. In addition, removal of the charged βAsp^{675} residue will reduce the negative electrostatic potential of this pore (13).

Based on these structural observations, we suggest that the amino acid changes at βD675 could affect either or both of the conformational changes associated with moving the NTP from the E to PS site and from the PS to A site. One possible scenario is a "double check" of fidelity. Transition from the E site to the PS site may function as the first check for fidelity. Specifically, the narrow pore through which the NTP rotates may serve as an electrostatic gate, checking the "fit" of the NTP into the PS site and rapidly rejecting NTPs that are very bad fits. The transition from the PS site to the A site may then serve as a second more stringent test of the identity of NTP by checking for Watson-Crick pairing before transition to the A site. Any mutation that makes the transition from either the E to PS site or the PS to A site more favorable could result in lower fidelity. These suggestions are consistent with the observation that the βD675Y mutant exhibits normal kinetics for correct incorporation because the correct base will be a "perfect" match, and these conformational changes are not likely to be rate-limiting for correct incorporation. In fact, recent data suggest that the rate-limiting step to correct incorporation may be phosphodiester bond formation (9).

This proposed two-step mechanism of nucleotide discrimination differs from those proposed for T7 RNA polymerase (14, 16, 17) and provides an explanation for the observation that wild-type multisubunit RNAPs are more discriminating toward the type of misincorporation events that occur than single subunit RNAPs and DNA polymerases (33–36). Wild-type *E. coli* RNAP only misincorporates UMP, not AMP or GMP, in place of CMP (23). Specifically, the transition of the NTP from the E to PS sites may be inhibited because the larger purine ring may not be able to fit through a pore designed to accommodate a pyrimidine. We tested the possibility that the βAsp^{675} mutants would permit AMP to be misincorporated for CMP and found that the mutants still discriminated against AMP incorporation (data not shown). This result suggests that mutation of βAsp^{675} is not sufficient to remove the discrimination of purines in place of pyrimidines.

We have characterized the correct and incorrect incorporation kinetics of four RNAP mutants, three of which have mutations in totally conserved residues (H673L, N620I/D814V, and R678C; Fig. 5). Interestingly, the kinetics of correct and incorrect incorporation are not significantly different from wild-type for these three mutants, whereas mutation of the semiconserved βAsp^{675} residue results in a significant decrease in the fidelity of nucleotide incorporation. To our knowledge, the βAsp^{675} mutants represent the first true fidelity mutants that have been identified for multisubunit RNAPs. In an early study, a fidelity mutant was characterized, but the mutated amino acid was not identified (37). Our data indicate that residues in the secondary channel are involved in nucleotide discrimination and are consistent with the NTPs entering through the secondary channel in the activated state, as we have previously suggested (26), although they do not rule out the possibility that the NTPs may enter through the main channel. Our kinetic data taken together with previous studies (6, 9, 11, 23) suggest a possible a three-step NTP binding model that permits a double check of the identity of the NTP before incorporation. Accordingly, we propose that the transitions of the NTP from the E site to the PS site and from the PS site to the catalytic (A) site both can be rate-limiting steps to misincorporation, and therefore, both transitions can govern nucleotide discrimination and fidelity.

REFERENCES

1. Zhang, G., Campbell, E. A., Minakhin, L., Richter, C., Severinov, K., and Darst, S. A. (1999) *Cell* **98,** 811–824
2. Cramer, P., Bushnell, D. A., and Kornberg, R. D. (2001) *Science* **292,** 1863–1876
3. Gnatt, A. L., Cramer, P., Fu, J., Bushnell, D. A., and Kornberg, R. D. (2001) *Science* **292,** 1876–1882
4. Cramer, P. (2004) *Adv. Protein Chem.* **67,** 1–42
5. Westover, K. D., Bushnell, D. A., and Kornberg, R. D. (2004) *Science* **303,** 1014–1016
6. Westover, K. D., Bushnell, D. A., and Kornberg, R. D. (2004) *Cell* **119,** 481–489
7. Korzheva, N., Mustaev, A., Kozlov, M., Malhotra, A., Nikiforov, V., Goldfarb, A., and Darst, S. A. (2000) *Science* **289,** 619–625
8. Vassylyev, D. G., Sekine, S., Laptenko, O., Lee, J., Vassylyeva, M. N., Borukhov, S., and Yokoyama, S. (2002) *Nature* **417,** 712–719
9. Temiakov, D., Zenkin, N., Vassylyeva, M. N., Perederina, A., Tahirov, T. H., Kashkina, E., Savkina, M., Zorov, S., Nikiforov, V., Igarashi, N., Matsugaki, N., Wakatsuki, S., Severinov, K., and Vassylyev, D. G. (2005) *Mol. Cell.* **19,** 655–666
10. Armache, K. J., Mitterweger, S., Meinhart, A., and Cramer, P. (2005) *J. Biol. Chem.*

280, 7131–7134
11. Kettenberger, H., Armache, K. J., and Cramer, P. (2004) *Mol. Cell.* **16,** 955–965
12. Campbell, E. A., Korzheva, N., Mustaev, A., Murakami, K., Nair, S., Goldfarb, A., and Darst, S. A. (2001) *Cell* **104,** 901–912
13. Batada, N. N., Westover, K. D., Bushnell, D. A., Levitt, M., and Kornberg, R. D. (2004) *Proc. Natl. Acad. Sci. U. S. A.* **101,** 17361–17364
14. Yin, Y. W., and Steitz, T. A. (2004) *Cell* **116,** 393–404
15. Cramer, P., Bushnell, D. A., Fu, J., Gnatt, A. L., Maier-Davis, B., Thompson, N. E., Burgess, R. R., Edwards, A. M., David, P. R., and Kornberg, R. D. (2000) *Science* **288,** 640–649
16. Landick, R. (2004) *Cell* **116,** 351–353
17. Temiakov, D., Patlan, V., Anikin, M., McAllister, W. T., Yokoyama, S., and Vassylyev, D. G. (2004) *Cell* **116,** 381–391
18. Burton, Z. F., Feig, M., Gong, X. Q., Zhang, C., Nedialkov, Y. A., and Xiong, Y. (2005) *Biochem. Cell Biol.* **83,** 486–496
19. Nedialkov, Y. A., Gong, X. Q., Hovde, S. L., Yamaguchi, Y., Handa, H., Geiger, J. H., Yan, H., and Burton, Z. F. (2003) *J. Biol. Chem.* **278,** 18303–18312
20. Gong, X. Q., Zhang, C., Feig, M., and Burton, Z. F. (2005) *Mol. Cell* **18,** 461–470
21. Zhang, C., Zobeck, K. L., and Burton, Z. F. (2005) *Mol. Cell. Biol.* **25,** 3583–3595
22. Santangelo, T. J., Mooney, R., Landick, R., and Roberts, J. W. (2003) *Genes Dev.* **17,** 1281–1292
23. Erie, D. A., Hajiseyedjavadi, O., Young, M. C., and von Hippel, P. H. (1993) *Science* **262,** 867–873
24. Uptain, S. M., and Chamberlin, M. J. (1997) *Proc. Natl. Acad. Sci. U. S. A.* **94,** 13548–13553
25. Burgess, R. R., and Jendrisak, J. J. (1975) *Biochemistry* **14,** 4634–4638
26. Holmes, S. F., and Erie, D. A. (2003) *J. Biol. Chem.* **278,** 35597–35608
27. Anderson, K. S., Sikorski, J. A., and Johnson, K. A. (1988) *Biochemistry* **27,** 7395–7406
28. Cramer, P. (2002) *Curr. Opin. Struct. Biol.* **12,** 89–97
29. Sosunov, V., Sosunova, E., Mustaev, A., Bass, I., Nikiforov, V., and Goldfarb, A. (2003) *EMBO J.* **22,** 2234–2244
30. Foster, J. E., Holmes, S. F., and Erie, D. A. (2001) *Cell* **106,** 243–252
31. Erie, D. A. (2002) *Biochim. Biophys. Acta* **1577,** 224–239
32. Artsimovitch, I., Chu, C., Lynch, A. S., and Landick, R. (2003) *Science* **302,** 650–654
33. Huang, J., and Sousa, R. (2000) *J. Mol. Biol.* **303,** 347–358
34. Doublie, S., Tabor, S., Long, A. M., Richardson, C. C., and Ellenberger, T. (1998) *Nature* **391,** 251–258
35. Johnson, K. A. (1993) *Annu. Rev. Biochem.* **62,** 685–713
36. Li, Y., Korolev, S., and Waksman, G. (1998) *EMBO J.* **17,** 7514–7525
37. Blank, A., Gallant, J. A., Burgess, R. R., and Loeb, L. A. (1986) *Biochemistry* **25,** 5920–5928